Materials Research Bulletin 44 (2009) 555–559

Contents lists available at ScienceDirect

Materials Research Bulletin

journal homepage: www.elsevier.com/locate/matresbu

Spark plasma sintering of $BiFeO_3$

R. Mazumder [a], D. Chakravarty [b], Dipten Bhattacharya [c], A. Sen [c,*]

[a] Department of Ceramic Engineering, National Institute of Technology, Rourkela 769008, India
[b] International Advanced Research Centre for Powder Metallurgy and New Materials (ARCI), Balapur P.O., Hyderabad 500005, India
[c] Sensor & Actuator Division, Central Glass and Ceramic Research Institute, Council of Scientific and Industrial Research, Kolkata 700032, India

ARTICLE INFO

Article history:
Received 23 May 2007
Received in revised form 16 June 2008
Accepted 15 July 2008
Available online 26 August 2008

Keywords:
A. Ceramics
D. Dielectric properties
D. Ferroelectricity

ABSTRACT

Dense $BiFeO_3$ ceramics were prepared by a novel spark plasma sintering (SPS) technique. The sintering was conducted at temperatures ranging from 675 to 750 °C under 70 MPa pressure. A bulk density value up to 96% of theoretical density was achieved in the process. This contrast to around 90% of the theoretical density achieved by conventional sintering at around 830 °C. It was found that the tendency to form unwanted $Bi_2Fe_4O_9$ phase is higher at a high sintering temperature for SPS. The dielectric and ferroelectric properties also improved (with respect to conventionally sintered sample) for spark plasma-sintered samples.

1. Introduction

The multiferroics with, at least, two of the three orders or degrees of freedom – (anti)ferromagnetic, (anti)ferroelectric, and ferroelastic – coexisting and often a coupling among them, are rare in nature as transition metal ions with active *d* electrons tend to reduce the off-center distortion necessary for ferroelectricity [1]. The co-existence of ferroelectricity and (anti)ferromagnetism and their coupling with elasticity provide an extra degree of freedom in the design of new functional sensors and multistate devices [2]. $BiFeO_3$ is the most interesting in the family of a very few single-phase multiferroics because of its high phase transition temperatures (Curie temperature ~1083 K and Neel temperature ~675 K) [3].

The major bottlenecks of making $BiFeO_3$ ceramics lie in: (i) synthesizing phase pure material and (ii) achieving sintered densities above 90% of the theoretical density. Several techniques have been employed in synthesizing phase pure $BiFeO_3$. In the solid state route [4], Bi_2O_3 and Fe_2O_3 are reacted at a temperature in the range of 800–830 °C and unreacted $Bi_2O_3/Bi_2Fe_4O_9$ phases are removed by washing in HNO_3. The disadvantages of this process lie in the necessity of leaching the unwanted phases using an acid and also in the formation of coarse powder. Another technique is to take recourse to simultaneously precipitaton/co-precipitaton [5], where a solution of bismuth and iron nitrates is treated with ammonium hydroxide to get a hydroxide precipitate. The precipitate needs calcination at a temperature in the range of 550–750 °C to get phase pure $BiFeO_3$. In another approach nanosized $BiFeO_3$ particles have been prepared by a solution evaporation (tartaric acid template) [6] technique at a temperature as low as 450 °C. Mazumder et al. [7] reported the results of a comprehensive study of the phase transition at T_N (Neel temperature) as a function of particle size, where $BiFeO_3$ powders were synthesized by sonochemical route, combustion synthesis and co-precipitation technique.

Incidentally, there are only a few reports of making densified and highly resistive $BiFeO_3$ ceramics. Kumar et al. [8] reported the dielectric and ferroelectric properties of $BiFeO_3$ ceramics, where $BiFeO_3$ was prepared by a solid state route. However, there was no report about the bulk densities of the samples and the spontaneous polarization of the samples was very low. Wang et al. [9] showed that a rapid liquid-phase sintering of $BiFeO_3$ can result in 92% of the theoretical density and gave rise to spontaneous and remanent polarization of 8.9 and 4.0 $\mu C/cm^2$, respectively. Pradhan et al. [10] followed a similar rapid phase sintering route, but the percent densification was not reported though the microstructure revealed poor densification resulting in low spontaneous and remanent polarizations values of 3.5 and 2.5 $\mu C/cm^2$, respectively. Recently, Yuan et al. [11] followed a rapid phase sintering technique and synthesized highly resistive and dense (92% of theoretical density) samples by varying the particle size of the precursors Bi_2O_3 and Fe_2O_3 and they reported a high spontaneous polarization of their samples.

* Corresponding author.
E-mail address: asen@cgcri.res.in (A. Sen).

0025-5408/$ – see front matter © 2008 Published by Elsevier Ltd.
doi:10.1016/j.materresbull.2008.07.017

Incidentally, grain coarsening and densification are two simultaneous processes during sintering and the ratio between them has a crucial influence on microstructure [12,13]. It is generally accepted that the enthalpy for surface diffusion (grain coarsening) in a material is lower than that for bulk diffusion (densification). In this case, there will be a high-temperature region for sintering where bulk diffusion is enhanced relative to surface diffusion and, thus, densification is favoured over grain coarsening. Rapid sintering is a technique allowing a very high heating rate at high temperatures which minimizes grain coarsening. Recently, spark plasma sintering (SPS) has got a lot of attention as a technique to fully densify metals and ceramics at a relatively low temperature and in a very short time (usually in a few minutes) [14,15]. It takes advantage of microscopic electrical discharges between particles under pressure when a pulsed dc current is applied. Its influences on mass transport can be attributed to one of the several intrinsic effects like the influence of an electric current on the diffusion rate [16], an increase in point defect concentration and a reduction in the activation energy for mobility of the defects.

In the present work, $BiFeO_3$ was densified by an SPS technique. The conventional sintering of $BiFeO_3$ was also conducted for comparison of properties. To the best of our knowledge, this is the first report on the characteristics of highly dense spark plasma-sintered $BiFeO_3$ ceramics.

2. Experimental

Pure $BiFeO_3$ powder was synthesized using a simultaneous precipitation route as described below. $Fe(NO_3)_3$ and $Bi(NO_3)_3$ solutions of 0.2 M concentration were mixed together and the mixed solution was then poured into aqueous ammonia under stirring and the pH was maintained at 9 for complete precipitation. The precipitate was filtered, dried at 100 °C in an oven for 6 h and calcined at 550 °C/1 h. The phase identification of the powder was performed by an X-ray diffractometer (Philips, PW 1710; Cu Kα radiation). Particle size was measured by Malvern Mastersizer 2000 particle size analyzer. DSC study was carried out in a PerkinElmer Diamond DSC over a temperature range of 27–550 °C. Pellets from the synthesized powder were prepared using uniaxial pressing at a pressure of 170 MPa. For conventional sintering, the pellets were sintered at 830 °C/2 h at a heating rate of 150 °C/h and cooled inside the furnace (samples designated CS). Spark plasma sintering was carried out using the model Dr. Sinter 1050 (Sumitomo Coal mining Co. Ltd., Japan). The calcined powder was poured in a cylindrical graphite die of 15 mm diameter, sintered in partial vacuum (6 Pa) for 10 min under a uniaxial pressure of 70 MPa applied throughout the sintering cycle. The sintering temperature was varied from 675 to 750 °C and the heating rate was kept constant at 250 °C/min. At the end of the soaking time the power and pressure were switched off and the samples were naturally cooled inside the chamber. The ground pellets were subjected to thermo-gravimetric analysis (Shimadzu) to determine the temperature of annealing. For maintaining oxygen stoichiometry, SPS-sintered samples need an annealing treatment at 650 °C for 2 h. The densities of the sintered pellets were measured by Archimedes' principles.

For the dielectric and resistivity measurements, the surfaces of the sintered pellets were ground and polished followed by application of a silver conducting paste on two opposite surfaces of the sample. The silver paste was then cured at 500 °C for 15 min. The dielectric measurements were performed at room temperature using Solartron impedance analyzer in the frequency range of 10 Hz to 10 MHz. Two-probe electrical resistance was measured by an HP 3458A multimeter from room temperature to 400 °C. Ferroelectric hysteresis loops were obtained using an LC precision ferroelectric tester.

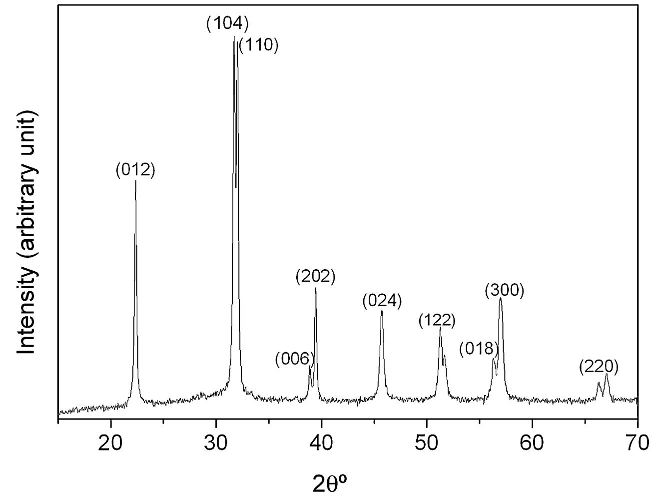

Fig. 1. X-ray diffraction pattern of calcined $BiFeO_3$ powder.

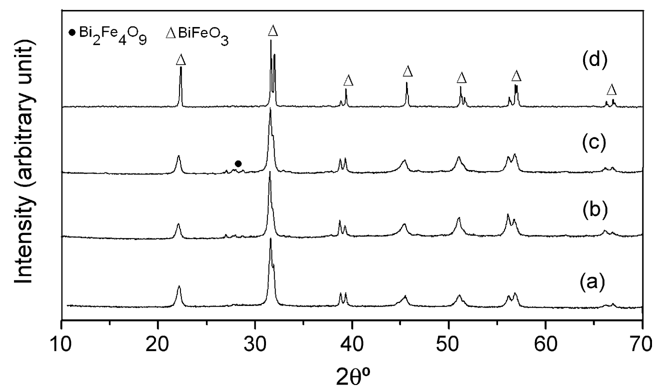

Fig. 2. X-ray diffraction patterns of ground SPS pellets after sintering at different temperatures (a) 675 °C, (b) 700 °C, (c) 750 °C and (d) conventionally sintered (CS) pellet (and ground 830 °C).

3. Results and discussion

The XRD pattern of the synthesized (and calcined) powder (Fig. 1) shows the presence of $BiFeO_3$ phase only. Fig. 2 shows the XRD traces of ground SPS pellets sintered at different temperatures [Fig. 2(a)–(c)] and pellets conventionally-sintered at 830 °C [Fig. 2(d)]. From the figures it is clear that in case of SPS, the higher sintering temperature generates an impurity phase

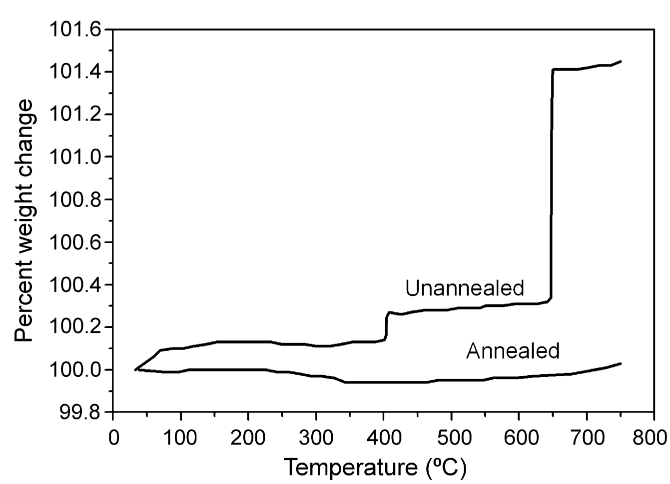

Fig. 3. TGA curves of as-sintered and annealed SPS samples.

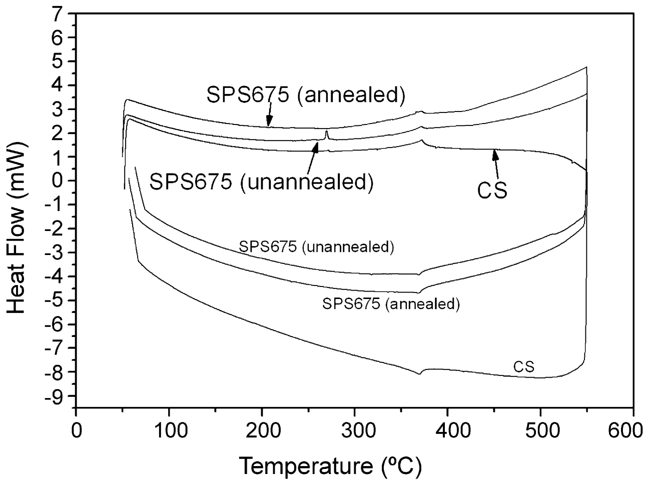

Fig. 4. Differential scanning calorimetry traces of an annealed and an unannealed SPS sample and a CS sample.

($Bi_2Fe_4O_9$). Incidentally, $BiFeO_3$ is a metastable compound, and during its synthesis, other compounds from the Bi_2O_3–Fe_2O_3 system often appear as impurities. The applied pressure, current and atmosphere during SPS may further lower the stability of $BiFeO_3$ leading to impurity phases at elevated temperatures. The SPS sample sintered at 675 °C (designated SPS675) was found to posses optimum properties along with phase purity. The TGA plot (Fig. 3) shows a weight gains of an as-sintered sample at around 400 and 650 °C confirming oxygen deficiency. The sample annealed in air at 650 °C show no such weight change. The weight gain may be due to oxidation of iron/bismuth of lower oxidation state. However, detailed studies are required to find out the reason behind the two step process of oxygen incorporation in the material. The differential scanning calorimetry trace (Fig. 4) of SPS675 (without annealing) showed two endothermic peaks at 270 and 375 °C, whereas, the annealed SPS sample and also the CS sample showed only one endothermic peak at 375 °C, the latter corresponds to antiferromagnetic to paramagnetic transition [3] of $BiFeO_3$. The reason behind the endothermic peak in the unannealed sample at 270 °C needs further probing. Fig. 5 shows the micrographs of the fracture surfaces of the samples prepared by the conventional and SPS technique. The density of CS sample was around 91% of the theoretical density (measured by Archimedes' principle), whereas SPS sample showed almost 96% of the theoretical density. For SPS675, the microstructure showed almost pore-free morphology with grain size slightly lower than that of CS sample. Fig. 6 shows the frequency dependent dielectric behavior of CS and SPS675 samples. The permittivity for SPS samples at high frequencies is higher than that of CS samples, which may be attributed to higher relative density (low porosity) of SPS ceramics, since, in general, porosity lowers the permittivity. Incidentally, the enhancement of dielectric constant at low frequency for CS (in contrast to SPS) is also associated with a high dielectric loss. Also the dielectric loss tends to increase without showing a peak at low

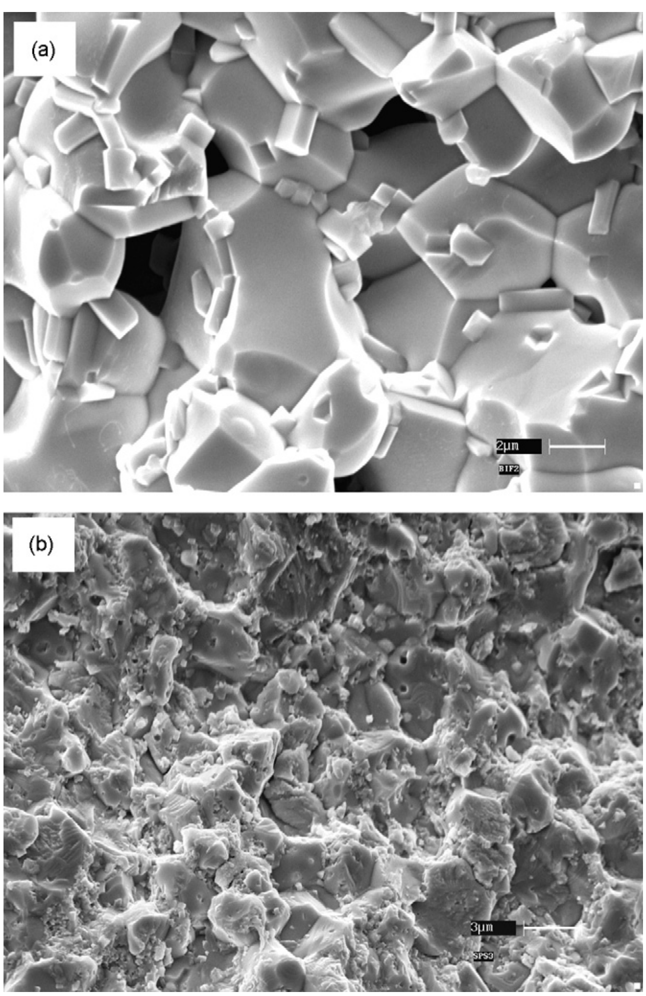

Fig. 5. SEM micrographs of fracture surfaces of (a) CS and (b) SPS675.

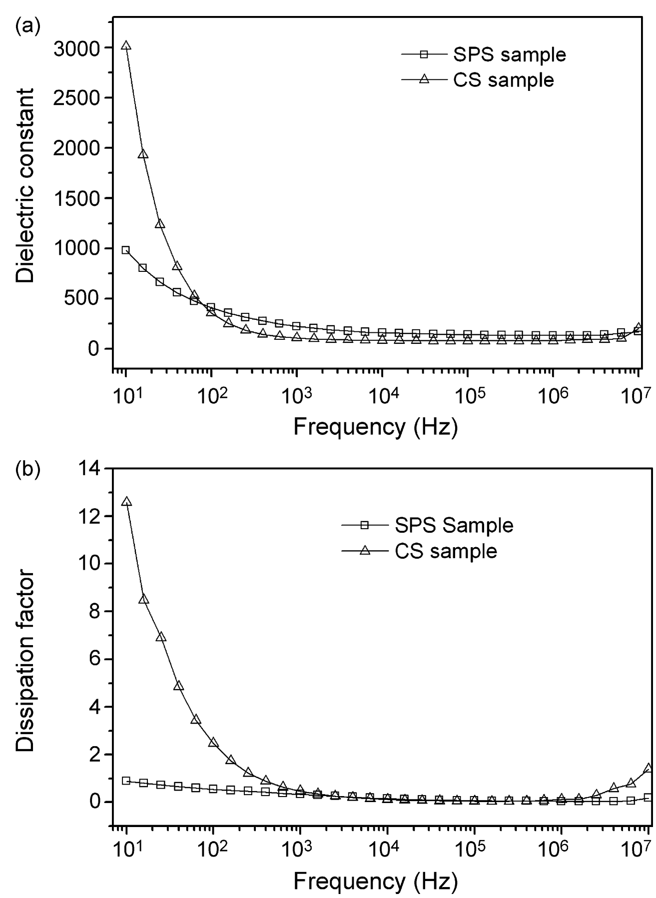

Fig. 6. Variation of (a) dielectric constant and (b) dissipation factor with frequency (at room temperature) for CS and SPS675 samples.

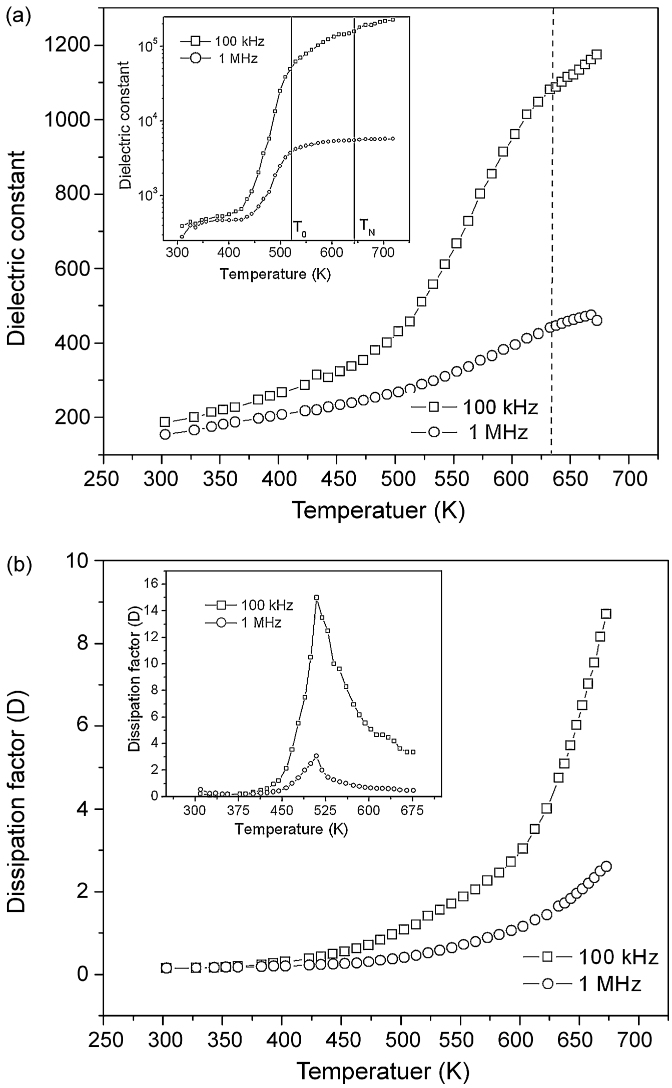

Fig. 7. (a) Dielectric permittivity and (b) dissipation factor vs. temperature for the SPS sample at 100 kHz and 1 MHz frequency (inset CS sample).

frequencies. This is a signature of Maxwell–Wagner type relaxation [17], which is the consequence of charge accumulation at the discontinuities/grain boundaries within the dielectrics. To understand this behavior, we have to first note that in $BiFeO_3$, small amounts of Fe^{2+} ions and oxygen vacancies exist [18]. Incidentally, $BiFeO_3$ shows [19] p-type conductivity, which can be understood by considering substitution of a small amount Fe^{2+} ions in Fe^{3+} positions (acceptor doping of Fe^{3+} by Fe^{2+}). The presence of free holes in sufficient concentration can give rise to Maxwell–Wagner relaxation which, is true for CS, because due to its higher firing temperature, the hole concentration should be more (as some Bi^{3+} ions are reduced to Bi^{2+} at a high temperature) with consequent dispersion at low frequency. Fig. 7 shows the temperature dependence of dielectric permittivity and dissipation factor for SPS675 sample (and the inset CS sample). The results indicate thermally activated dissipation process. The CS sample exhibited two anomalies—at T_o (onset of magnetic transition) and T_N (Neel temperature) over a temperature span (ΔT) of $\sim$100 K. The two anomalies across ΔT – instead of only one at T_N – result from the broadening of the magnetic transition due to inhomogenity and the details have been given elsewhere [7]. An inflection point was observed for SPS675 sample at 650 K in the dielectric constant curve. It appears to be closely related to a phase transition from the antiferromagnetic to paramagnetic phase. Fig. 8 shows the temperature dependence of dc conductivity for $BiFeO_3$ samples and it is found that the dc conductivity (σ_{dc}) obeys a thermally activated Arrhenius type behavior:

$$\sigma_{dc} = \sigma_0 \exp\left(\frac{-\Delta E}{kT}\right) \tag{1}$$

It is observed that the conductivity increases with the increase in temperature and shows a slight change in slope in the temperature region 523–673 K. This change in slope may be related to the change in conductivity mechanism. The activation energies in the low-temperature range (373–523 K) and high-temperature range (523–673 K) are 0.4238 and 0.3353 eV, respectively. For SPS675 sample the room temperature resistivity is 82 MΩ cm, whereas for the CS sample the same is 7.2 MΩ cm indicating the high resistance nature of the SPS samples. The inset of Fig. 8 shows the log dc resistivity vs. $1/T$ trace for the CS sample. The activation energies calculated from the data turn out to be 0.88 and 0.19 eV below T_o and above T_o, respectively.

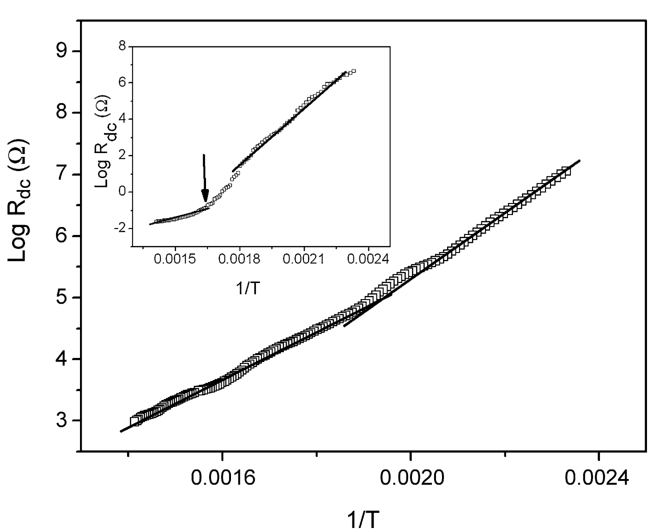

Fig. 8. log R_{dc} vs. inverse absolute temperature plot for SPS675 sample (inset for the CS sample).

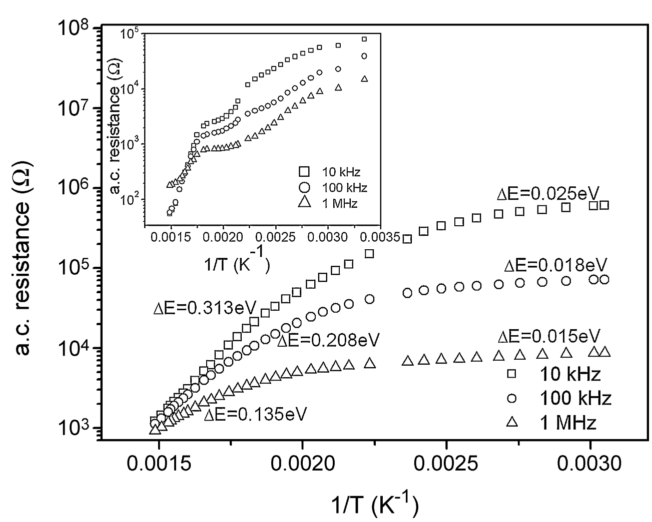

Fig. 9. ac resistance vs. inverse absolute temperature plots for SPS675 sample at different frequencies and (inset CS sample).

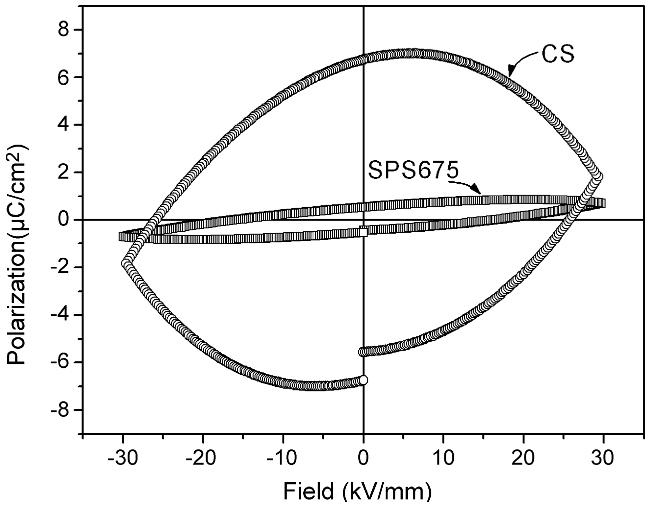

Fig. 10. *P–E* hysteresis loops of CS and SPS675 samples.

Fig. 9 shows the ac conductivity plots at different frequencies for SPS samples. It is observed from these plots that in the low-temperature regime, ac conductivity increases with the increase in frequency. The activation energy values increase with the increase in temperature. Further work is needed to understand this behavior. Incidentally, the dc conductivity of the samples is a few orders of magnitude lower than the ac conductivity and its nature of variation with temperature is also different. This is expected because dc conductivity is determined by the most difficult transition in complete percolation paths between the electrodes, while ac conductivity is determined by the easiest local movement of the charges. At higher temperatures dc and ac resistivity values become closer. The inset of Fig. 9 shows the ac conductivity of the CS sample. Below 570 K it shows a non-linear behavior and cannot be fitted to Arrhenius equation. Above 570 K it shows almost a linear behavior and the activation energies are 0.5, 0.43 and 0.19 eV at 10 kHz, 100 kHz and 1 MHz, respectively.

Fig. 10 shows the *P–E* loops of CS and SPS samples. The leakage current in low-resistive CS sample was high as supported from the lossy hysteresis loop. On the other hand, the leakage current in the SPS sample was very low in comparison to the CS sample. However, both CS and SPS samples failed to reach the saturated polarization before the leakage currents became significant.

4. Conclusion

Highly resistive $BiFeO_3$ sample was prepared by SPS technique. The sintered density was higher compared to that of conventionally sintered samples. The SPS samples also showed low dielectric dispersion and high resistivity.

Acknowledgements

One of the authors (R.M.) is thankful to CSIR, India for financial support. We are grateful to Dr. G. Sundararajan, Director, ARCI, Hyderabad for permitting us to use the Spark Plasma Sintering facility. We also thank Director, CGCRI for giving permission to publish this paper.

References

[1] H. Schmid, Ferroelectrics 162 (1994) 317.
[2] N.A. Hill, J. Phys. Chem. B 104 (2000) 6694.
[3] J. Wang, J.B. Neaton, H. Zheng, V. Nagarajan, S.B. Ogale, B. Liu, D. Viehland, V. Vaithyanathan, D.G. Schlom, U.V. Waghmare, N.A. Spaldin, K.M. Rabe, M. Wuttig, R. Ramesh, Science 299 (2003) 1719.
[4] G.D. Achenback, W.J. James, R. Gerson, J. Am. Ceram. Soc. (1967) 437.
[5] S. Shetty, V.R. Palkar, R. Pinto, Pranama J. Phys. 58 (2002) 1027.
[6] S. Ghosh, S. Dasgupta, A. Sen, H.S. Maiti, J. Am. Ceram. Soc. 88 (2005) 1349.
[7] R. Mazumder, S. Ghosh, P. Mondal, D. Bhattacharya, S. Dasgupta, N. Das, A. Sen, A.K. Tyagi, M. Sivakumar, T. Takami, H. Ikuta, J. Appl. Phys. 100 (2006) 033908.
[8] M.M. Kumar, V.R. Palkar, K. Srinivas, S.V. Suryanarayana, Appl. Phys. Lett. 76 (2000) 2764.
[9] Y.P. Wang, L. Zhou, M.F. Zhang, X.Y. Chen, J.-M. Liu, Z.G. Liu, Appl. Phys. Lett. 84 (2004) 1731.
[10] A.K. Pradhan, Kai Zhang, D. Hunter, J.B. Dadson, G.B. Loiutts, P. Bhattacharya, R. Katiyar, J. Zhang, D.J. Sellmyer, J. Appl. Phys. 97 (2005) 093903.
[11] G.L. Yuan, S.W. Or, Y.P. Wang, Z.G. Liu, J.M. Liu, Solid State Commun. 138 (2006) 76.
[12] S.M. Landin, W.A. Schulze, J. Am. Ceram. Soc. 73 (1990) 913.
[13] M.P. Harmer, R.J. Brook, J. Br. Ceram. Soc. 80 (1981) 147.
[14] B.-P. Zhang, J.-F. Li, K. Wang, H. Zhang, J. Am. Ceram. Soc. 89 (2006) 1605.
[15] T. Wada, K. Tsuji, T. Saito, Y. Matsuo, Jpn. J. Appl. Phys. 42 (2003) 6110.
[16] N. Bertolino, J. Garay, U. Anselmi-Tamburini, Z.A. Munir, Scripta Mater. 44 (2001) 737.
[17] D. O'Neill, R.M. Bowman, J.M. Gregg, Appl. Phys. Lett. 77 (2000) 1520.
[18] V.R. Palkar, R. Pinto, Pramana J. Phys. 58 (2002) 1003.
[19] A.S. Poghossian, H.V. Abovian, P.B. Avakian, S.H. Mkrtchian, V.M. Haroutunian, Sens. Actuators B 4 (1991) 545.